Estimation of 3D Instantaneous Motion of a Ball from a Single Motion-Blurred Image

Giacomo Boracchi, Vincenzo Caglioti, and Alessandro Giusti

Dipartimento di Elettronica e Informazione,
Politecnico di Milano, Via Ponzio, 34/5 20133 Milano
giacomo.boracchi@polimi.it, vincenzo.caglioti@polimi.it,
alessandro.giusti@polimi.it

Abstract. We present a single-image algorithm for reconstructing the 3D velocity, the 3D spin axis, and the angular speed of a moving ball. Peculiarity of the proposed algorithm is that this reconstruction is achieved by accurately analyzing the blur produced by the ball motion during the exposure. We combine image analysis techniques in order to obtain 3D estimates, that are then integrated into a geometrical model for recovering the 3D motion.

The algorithm is validated with experiments on both synthetic and camera images. In a broader scenario, we exploit this specic problem for discussing motivations, advantages, and limitations of reconstructing 3D motion from motion blur.

1 INTRODUCTION

In this paper we propose a technique for estimating the 3D motion of a ball from a single motion blurred image. We consider the instantaneous ball motion, which is described by a composition of 3D velocity and spin around a 3D axis: the proposed technique estimates both these components by analyzing motion blur.

Our approach differs from a more traditional and intuitive method consisting in recovering motion by analyzing successive video frames: the expected shortcomings of such *modus operandi* in realistic operating conditions motivate our peculiar approach. In fact, depending on equipment quality, lighting conditions and ball speed, a moving ball often results in a blurred image. Feature matching in successive video frames becomes very challenging because of motion blur and also because of repetitive features on the ball surface: this prevents *inter-frame* ball spin recovery. Then, it is worth considering *intra-frame* information carried by the motion blur. Our single-image approach has the further advantage of enabling the use of cheap, high-resolution consumer digital cameras, which currently provide a much higher resolution than much more expensive video cameras. High resolution images are vital for performing accurate measurements as the ball usually covers a small part of the image.

In this paper, we use an alpha matting algorithm (see Section 3.1) in order to separate the blurring effects produced by the ball translation from those

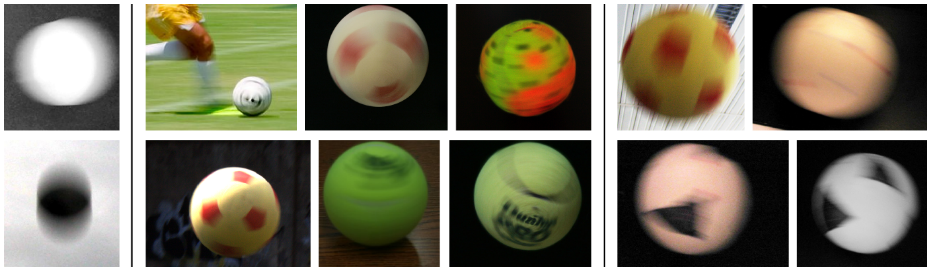

Fig. 1. Some blurred ball images. Leftmost images are textureless, so their spin can not be recovered. Central images show textured balls whose spin component dominates the apparent translation. Rightmost images are the most complete case we handle, showing a significant amount of apparent translation and spin; note that the ball contours also appear blurred in this situation, whereas they are sharp in the spin-only case.

produced by the ball spin. The ball 3D translation is then estimated using the techniques introduced in [1]; once the ball position and velocity are known, we analyze the blur smears on the blurred image surface, as introduced in [2]. Both these algorithms exploit the constraints derived from the geometry of the observed scene, and allow us to estimate the ball instantaneous motion, recovering 3D information from a single image.

The blur model derived from the 3D ball motion is presented in Section 2, while in Section 3 we briefly recall the image analysis algorithms used. The proposed technique is described in Section 4. Section 5 presents experimental results and Section 6 concludes with a broader discussion on motion estimation from blurred images.

1.1 Related Works

Given a single blurred image, the most treated problem in literature is the estimation of the point spread function (PSF) that corrupted the image [3–5], usually with the purpose of image restoration (*deblurring*).

Our work, on the contrary, takes advantage of motion blur for performing measurements on the imaged scene. Several other works follow a similar approach, such as [6], which describes a visual gyroscope based on rotational blur analysis, or [7], which estimates the scene depth map from an image acquired with a coded aperture camera. Also, [8] proposes to estimate the optical flow from a single blurred image. A ball speed measurement method based on a blurred image has been proposed in [9]. This assumes a simplified geometrical model that originates space-invariant blur and prevents the estimation of 3D motion and spin.

On the other hand, the problem of estimating the motion of a ball in the 3D space has been extensively treated in video tracking literature [10–12]. These methods assume the ball visible from multiple synchronized cameras, in order to triangulate the ball position in the corresponding frames. In [13] a method is proposed for reconstructing the ball 3D position and motion from a video sequence by analyzing its shadow. In [14, 15], a physics-based approach is adopted, to estimate the parameters of a parabolic trajectory. Recently, a technique for estimating the 3D ball trajectory from a single long exposure image has been presented in [16].

2 PROBLEM FORMULATION

Let S be a freely moving ball centered in C, whose radius R is known[1], imaged by a calibrated camera. The ball instantaneous motion, which is assumed constant during the exposure time $[0, T]$, is given by the composition of two factors:

- a linear translation with uniform velocity, $\mathbf{u}$. The translation distance during the exposure is therefore $T \cdot \mathbf{u}$.
- the spin around a 3D rotation axis a passing through C, with angular speed ω. The rotation angle which occurs during the exposure is therefore $T \cdot \omega$.

We further assume that the ball projections at the beginning and at the end of the exposure significantly overlap. Moreover, in order to recover the rotation axis and speed, we also require that spin is not too fast nor too slow w.r.t. the exposure time: $\pi/50 < \omega \cdot T < \pi/2$. In practice, these constraints allow us to use an exposure time $5 \div 10$ times longer than the exposure time which would give a sharp image. We assume that the blur on pixels depicting the ball is only due to ball motion. In practice, the distance between the ball and the camera is close to the focusing distance of the camera.

Our goal is to estimate the ball spin (both a and ω), velocity $\mathbf{u}$, and initial position by analyzing a single blurred image. The imaging model, underlying our analysis, is described in the sequel.

2.1 Blurred Image Formation

The blurred image Z can be modeled as the integration of infinitely many (sharp) sub-images $I_t, t \in [0, T]$, each depicting the ball in a different 3D position and spin angle (see Figure 2):

$$Z(x) = \int_0^T I_t(x)dt + \eta(x), \quad x \in X. \tag{1}$$

Where x represents the 2D image coordinates, $I_t(x)$ is the light intensity that reaches the pixel x at time t, and $\eta \sim N(0, \sigma^2)$ is white gaussian noise.

The ball apparent contours $\gamma_t, t \in [0, T]$ vary depending on translation only. Note that each apparent contour γ_t is an ellipse and that, in each sub-image I_t, γ_t may have a different position and also a different shape because of perspective

[1] if the radius is not known, the whole reconstruction can be performed up to a scale factor

Fig. 2. Blurred image formation model. The blurred image Z is obtained as the temporal integration of many still images I_t. The alpha map α of the blurred ball represents the motion of the object's contours and is used for recovering the translational motion component.

effects. In particular, $\gamma_{t=0}$ and $\gamma_{t=T}$ represent the ball at the beginning (*first curtain*) and at the end (*second curtain*) of the exposure, and will be named respectively γ_b and γ_e from now on. In our reconstruction procedure, we exploit the fact that the spin does not affect $\gamma_t\,, t \in [0, T]$, and thus the alpha map α is only determined by how γ_t changes during the exposure. The ball spin, combined with the translation, changes the depicted ball surface in each sub-image I_t, and obviously the appearance of the ball in Z.

2.2 Blur on the ball surface

We approximate the blur on the ball surface as locally space invariant [17]. In particular we approximate the blur in a small image region as the convolution of the sub-image I_0 with a PSF having vectorial support and constant value on it. Hence for any pixel x_i belonging to the ball image, we consider a neighborhood U_i of x_i and a PSF h_i such that

$$Z(x) \approx \int_X h_i(x - s) I_0(s) ds + \eta(x)\,,\ \forall x \in U_i \tag{2}$$

The PSF h_i is identified by two parameters, the direction θ_i and the extent l_i.

3 IMAGE ANALYSIS

We briefly introduce the main image analysis techniques used in this work.

3.1 Alpha Matting

Alpha matting refers to the procedure leading from an image to its alpha map, α. For each pixel x we have $\alpha(x) = 1$ if x is only affected by the foreground, $\alpha(x) = 0$ if x is a background pixel, and $0 < \alpha(x) < 1$ if x is a *mixed pixel*, i.e. a pixel whose intensity is affected by both the foreground and the background, such as along the object's border or in semitransparent areas.

In the general case the matting problem is under-constrained, even when the background is known. Still, in literature many algorithms have been proposed: some of them [18, 19] require a specific background (*blue screen matting*), whereas others, with minimal user assistance, handle unknown backgrounds (*natural image matting*) and large zones of mixed pixels ($0 < \alpha < 1$). Although none of these methods is explicitly designed for the interpretation of motion blurred images, alpha matting techniques have been recently applied to motion blurred images with different purposes, including point spread function (PSF) estimation [5] and blurred smear interpretation [20]. As shown in [21], by applying alpha matting to the motion-blurred image of an object we obtain a meaningful separation between the apparent motion of the object's boundaries (alpha map) and the actual blurred image of the object (color map).

It turns out that in the present scenario the alpha map of a blurred ball is not influenced by the spin but only by the translation: in practice, the alpha map is the image we would obtain if the background was black and the ball had a uniformly-white projection. In another interpretation, the alpha value at each pixel represents the fraction of the exposure time during which the ball image covered the pixel. Therefore the alpha map of the blurred ball is used to estimate the 3D ball position and velocity vector $T \cdot \mathbf{u}$ as described in Section 4.2. On the contrary, the foreground map only shows the blurred ball image, as if it was captured over a black background.

3.2 Blur Analysis

As mentioned in Section 2.2, we approximate the blur as locally shift invariant, produced by a convolution with a PSF having vector-like support. We estimate the blur direction and extent separately on N image regions $U_i \quad i = 1, .., N$ containing pixels which have been covered by the ball during the entire exposure time, i.e. $\alpha(x) = 1 \quad \forall x \in U_i,\ i = 1, .., N$.

We adapt the method proposed by Yitzhaky *et al* [22] for estimating the direction and extent of blur smears by means of directional derivative filters. The PSF direction within each U_i is estimated as the direction of the derivative filter d_θ having minimum energy response

$$\theta_i = \arg \min_{\theta \in [0,\pi]} \sum_{x_j \in U_i} w_j \big((d_\theta \circledast Z)(x_j)\big)^2 , \tag{3}$$

where $\circledast$ denotes the 2D convolution and w is a window function that determines U_i. Equation (3) is motivated by the fact that the blur removes all the details and attenuates the edges of I_0 along blur direction, and thus the blur direction can be determined by the directional derivative filter having minimum energy response. After estimating the PSF direction, its extent is obtained from the distance between two negative peaks in the autocorrelation of directional derivatives along the blur direction. Figure 3 shows some square regions used for blur analysis.

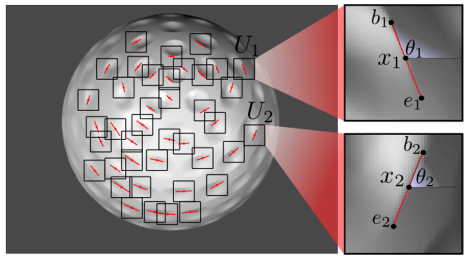

Fig. 3. A synthetic image of a spinning golf ball. U_i neighborhoods and recovered blur directions and extents are shown. Each segment $\overline{b_i e_i}$ represents the blur parameters θ_i, l_i within the region.

4 RECONSTRUCTION TECHNIQUE

For clarity purposes we illustrate the proposed technique first in the simpler case, where blur is due to ball spin only. Then, in Sections 4.2 and 4.3 we cope with the most general case where the ball simultaneously translates and spins.

4.1 Null Translation

Let us assume that during the exposure the ball does not translate, i.e. $\mathbf{u} = 0$, so that, in the blurred image, the ball apparent contour is sharp. The ball apparent contour γ is an ellipse and it allows us to localize the ball in the 3D space by means of the camera calibration parameters and knowledge of the ball radius. Points belonging to γ can be easily found in the image either by ordinary background subtraction or by extracting edge points in the alpha matte. We determine then γ by fitting an ellipse to such points, enforcing the projective constraint of being the image of a sphere captured from the calibrated camera.

Then, as described in Section 3.2, the PSF direction and extent are estimated within N regions $U_i, \quad i = 1, .., N$ contained inside γ. In order to avoid uniform-color areas, we select such regions around local maxima $x_i, i = 1, .., N$ of the Harris corner measure [23].

Such directions allows us to recover the 3D motions $\mathbf{v}_i$ of the ball surface at points corresponding to each of the regions. Since the camera is calibrated and the 3D position of the sphere S is known, we can backproject each pixel x_i on the sphere surface. Let X_i be the intersection point, closest to the camera, between the viewing ray of x_i and sphere S: the 3D motion direction of the ball surface at X_i is described by an unit vector $\mathbf{v}_i$ (see Figure 4 left). More precisely, let π_i be the plane tangent to S at X_i: then, $\mathbf{v}_i$ is found as the direction of the intersection between π_i and the viewing plane of the image line passing through x_i and having direction θ_i.

As shown in Figure 4 (left), all the vectors $\mathbf{v}_i \quad i = 1, .., N$ must lie on the same plane, orthogonal to the rotation axis a. Then, let $W = [\mathbf{v}_1|\mathbf{v}_2|..|\mathbf{v}_N]$, be the matrix having vectors $\mathbf{v}_i$ as columns. The direction of a is found as the

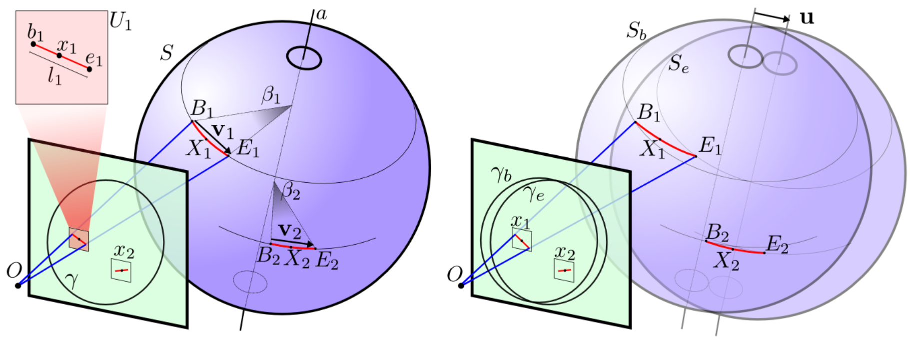

Fig. 4. Left: reconstruction geometry for zero translation. Right: reconstruction for full motion case.

direction of the eigenvector associated to the smallest of W's eigenvalues. This estimate is refined by iterating the procedure after removing the $\mathbf{v}_i$ vectors that deviate too much from the plane orthogonal to a (outliers).

Note that, when the ball is not translating, the ball apparent contour γ is sharp and in this case it is easily localized by fitting an ellipse to image edge points (possibly after background subtraction) or by using a generalized Hough transform, without need of alpha matting.

Although the rotation axis can be recovered exploiting θ_i directions only, in order to estimate the angular speed we need to consider also the blur length l_i estimated within regions U_i. Each of these extents represents the length of the trajectory (assumed rectilinear) that the feature traveled in the image during the exposure. For each feature, a starting point b_i and ending point e_i are determined in the image as

$$b_i = x_i - \frac{l}{2} \cdot \begin{pmatrix} \cos\theta \\ \sin\theta \end{pmatrix} \; e_i = x_i + \frac{l}{2} \cdot \begin{pmatrix} \cos\theta \\ \sin\theta \end{pmatrix} \tag{4}$$

and backprojected on the sphere surface S to points B_i and E_i, respectively. We then compute the dihedral angle β_i between two planes, one containing a and B_i, the other containing a and E_i. Such angles are computed only for those estimates not previously discarded as outliers. The spin angle is estimated as the median of the β_i angles. If the exposure time T is known, the spin angular speed ω immediately follows.

4.2 Recovering the Ball 3D Position and Velocity

The ball 3D position and the 3D velocity vector are recovered from the alpha map by estimating the ellipses γ_b and γ_e, the apparent contours of the ball at the beginning and at the end of the exposure.

Apparent Translation Direction Estimation The apparent translation direction corresponds to the projection on the image plane of the translation vector $\mathbf{u}$. When perspective effects are negligible, the blur in the alpha map is space invariant and can be expressed as a convolution of a binary alpha map against a PSF. Thus, the apparent translation direction of the ball can be estimated by applying Equation (3) to the alpha map of the whole image. However, because of the perspective effects the blur becomes space variant and the PSF directions point at the vanishing point of $\mathbf{u}$. In this case the PSF directions are nearly symmetric w.r.t. to the apparent translation direction and, when the eccentricities of γ_b and γ_e are small compared to the apparent displacement, Equation (3) returns sufficiently accurate estimates.

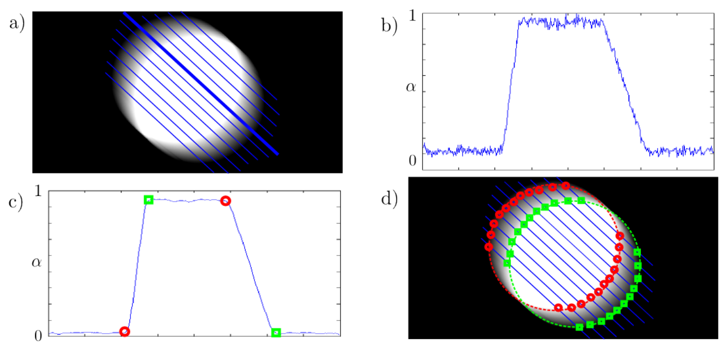

Fig. 5. Intensity profiles along directions approximately parallel to the blur direction in the image have similar characteristics.

Profile Analysis The procedure used to determine γ_b and γ_e is based on an analysis of the alpha map values along lines (*profiles*) parallel to the apparent translation direction. We consider n profiles, as illustrated Figure 5a, and on each profile we estimate the point these profiles intersects γ_b and γ_e.

Because of inaccuracies in the alpha map (see Figure 5b), these intersections can not be estimated as the end points of the segments having $\alpha = 0$ and $\alpha = 1$. Thus, we apply the iterative procedure described in [1] that is meant for monochromatic balls on uniform colored background and has been designed to cope with noise and shading. It exploits profile denoising and robust fitting of a linear model for the alpha values of pixels within semi-transparent areas; the result of such procedure on the profile in Figure 5b is illustrated in Figure 5c.

3D Reconstruction Once $2 \cdot n$ points belonging to each of γ_b and γ_e have been recovered from the n intensity profiles, these ellipses are estimated by conic fitting (Figure 5d). In order to reduce the degrees of freedom of the fitting procedure, we enforce that such ellipses are projections of a sphere (see [1]).

Since γ_b and γ_e are now known, the 3D ball position at the beginning and end of the exposure can be easily reconstructed by means of basic projective geometry, provided that the sphere radius is known and the camera is calibrated. The vector connecting their centers is the 3D displacement occurred during the exposure: this allows us to compute the absolute speed of the ball whenever the exact exposure time Δt is known (which is often the case).

4.3 Recovering Spin in the General Case

In order to account for the change in the ball's position, the procedure for spin estimation described in 4.2 is modified as follows (see Figure 4 right).

At first, the ball 3D displacement during the exposure is computed from the alpha map as described in section 4.1; this returns two spheres S_b and S_e having centers C_b and C_e respectively, representing the ball position at the beginning and end of the exposure.

Blur is then analyzed within image regions $U_i,\ i = 1,..,N$ whose pixels x satisfy the condition $\alpha(x) = 1$, i.e. pixels which have been covered by the ball during the whole exposure. For each U_i, image points b_i and e_i are returned, exactly as described in Section 4.1.

Unfortunately, in this case backprojecting the blur direction on the sphere is meaningless, since blur is caused by simultaneous translation and spin. Therefore, the viewing ray of b_i is intersected with S_b, which identifies a 3D point B_i and similarly, e_i is backprojected on S_e to find E_i (see Figure 4 (right)).

For each region, the 3D vector

$$\mathbf{v}_i = (E_i - B_i) - (C_e - C_b) \tag{5}$$

represents the 3D motion of the ball surface at the corresponding point, due to the spin component only. The spin axis a and angular velocity ω are now estimated as in the previous case.

The Orientation Problem Every motion recovered from blur analysis has an orientation ambiguity. This holds for the ball motion, and also for the blur direction estimates θ_i. The ambiguity is explained by Equation (1) where the blurred image is given by an integration of several sub-images: obviously, information about the order of sub-images is lost.

In the ball localization step we arbitrarily choose which of the two fitted ellipses is γ_b, representing the ball at the beginning of the exposure, and which is γ_e. But when each blurred feature x_i is considered and its endpoints b_i, e_i identified, there is no way to determine which corresponds to the feature location at the beginning of the exposure. Now the choice is not arbitrary since each must be backprojected to the correct sphere (S_b and S_e, respectively).

We propose the following possible criteria for solving the problem:

– if translation dominates spin, which is often the case in practical scenarios, blurred features should be oriented in the direction of the translational motion; our experimental validation uses this criterion.

– blur orientations in nearby regions should be similar;
– for features having one endpoint outside the intersection area between γ_b and γ_e only one orientation is consistent.

Another solution is computing the two possible vectors $\mathbf{v}'_i$ and $\mathbf{v}''_i$ for each feature, then using a RANSAC-like technique to discard the wrong ones as outliers.

5 EXPERIMENTS

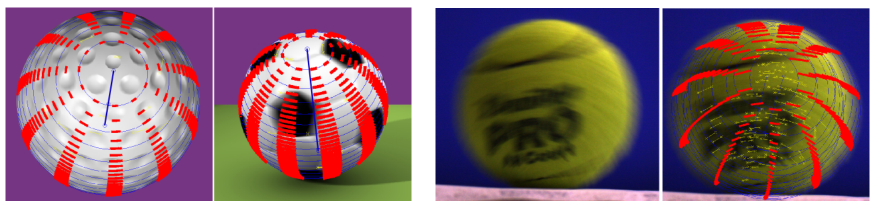

(a) (b)

Fig. 6. *(a)* Reconstruction results on two synthetic images (spin only). *(b)* A real image (tennis ball) spinning and translating, and reconstructed motion (right). Note complex motion of points on the ball surface due to simultaneous spin and translation: red stripes show reconstructed motion, and correctly interpret the observed blur. Since the ball was rolling on a table (bottom of the image), features on the bottom of the ball are correctly estimated as still, and the rotation axis as coplanar with the table.

We validated our technique on both synthetic and camera images. Each synthetic image has been generated according to Equation (1), by using the Blender 3D modeler [24] for rendering hundreds of 800×600 sharp frames with intensity values in $[0, 255]$. Each frame depicts the moving ball in a different time instant and corresponds to a sub-image I_t; the blurred image Z is given by the average of all these sub-images to which a Gaussian white noise is added. In our experiments we consider the spin angle $\omega \cdot T \in [1°, 20°]$ and the noise standard deviation $\sigma = 0, .., 3$, both in the spin-only and in the spin-plus-translation cases. Several scenarios (some of them are shown in Figures 6(a) and 7) have been rendered by varying the spin axes w.r.t to the camera position. In some cases we use a plain texture on the ball surface, whereas others feature a realistic ball surface with 3D details such as bumps, seams, and specular shading; these affects the blur on the ball surface, resulting in more difficult operating conditions. The PSF parameters are estimated form the corresponding grayscale images within disk shaped regions, whose radius increases from 30 to 45 pixels according to the noise standard deviation σ (which is estimated using [25]).

Table 1 presents the algorithm performance for estimating ω in the spin only case; some of these test images are shown in Figure 7. As one can see the algorithm accuracy decreases for low spin, as the low resolution of the image

Table 1. Mean relative error in ω estimation, expressed as a percentage w.r.t the true value of ω. Columns where $\sigma > 0$ shows the average over ten noise realizations.

$\omega \cdot T \ \backslash \ \sigma$	0	1	2	3
5.00	4.31	4.6222	5.0641	3.9401
6.25	2.26	2.5562	4.7898	4.3915
7.50	2.40	3.1353	2.7236	2.0544
8.75	0.75	1.5163	2.9408	5.0431
10.00	2.15	3.3975	5.3916	11.3800

does not allow reliable PSF estimation within small regions U_i. Figures 8 and 9 show the results on some camera images depicting several spinning balls. Both in synthetic and camera images, the blur estimates show a variable percentage of outliers ($5\% \div 50\%$), which are correctly discarded in most cases. This percentage is higher in noisy images, in images with smaller spin amounts and in images presenting texture with pronounced edges. Finally, we found that, in general, estimating the PSF extents is much more error-prone than estimating the PSF directions, without significant differences between real and synthetic images. This, combined with the orientation problem (see Section 4.3), makes the analysis of the spin-plus-translation, in general, a much more challenging case than the spin-only case (where the extents are used only to estimate $\omega \cdot T$).

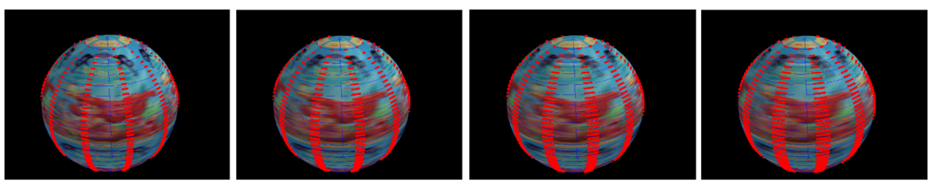

Fig. 7. Synthetic (spin only) image of textured ball at different ω values. From left to right $\omega \cdot T = 5°; 6.875°; 8.125°; 10°$

In order to overcome such issues in the general case, we also developed a user-assisted technique, which can be applied when the ball surface is pigmented with well-defined shapes; then, relevant information about the scene evolution can be visualized from the image of the second derivatives, which in our case clearly shows the initial and final contours of the ball, as well as any clear edges in the ball texture both at the beginning and at the end of the exposure [20]. An application of this user-assisted technique is shown and detailed in Figure 10.

6 DISCUSSION AND CONCLUSIONS

We proposed a technique for reconstructing the 3D position, velocity and spin of a moving ball from a single motion-blurred image, highlighting advantages

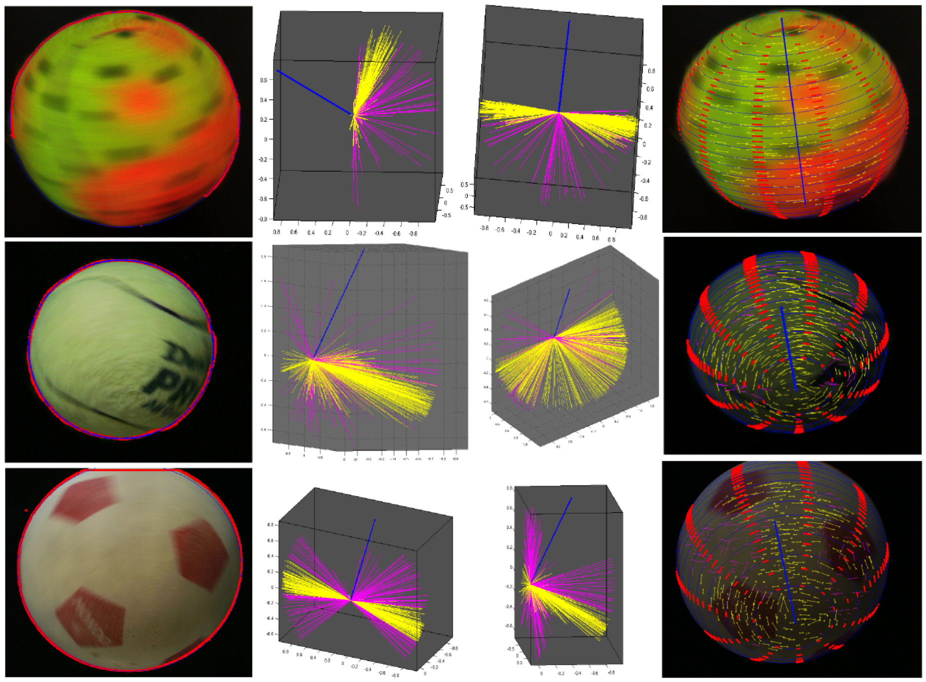

Fig. 8. Real images (spin only). Central columns shows axis (blue) and $\mathbf{v}_i$ directions from different viewpoints: yellow ones are inliers, magenta are outliers. Corresponding blur estimates are shown in the rightmost image as yellow segments. Reconstructed spin axes and speeds correctly explain the blurred image: for example, the spin axis passes through the sharpest parts of the ball image.

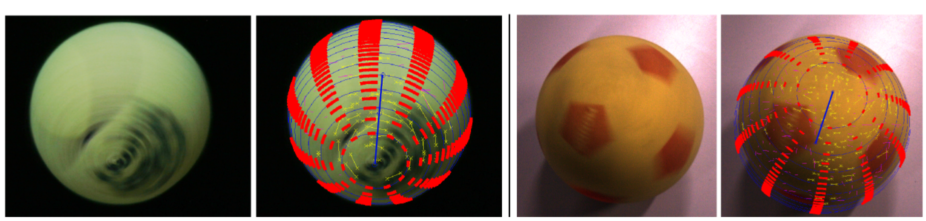

Fig. 9. Other real images, and reconstructed motions (spin only). Display colors are the same as in previous figures.

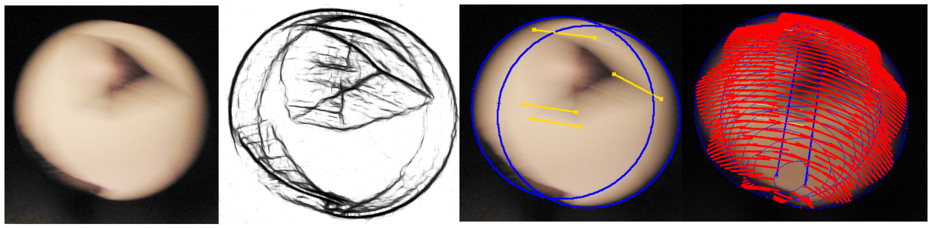

Fig. 10. Results after the user-assisted technique for recovering both translation and spin; a double differentiation of the original image highlights γ_b and γ_e, as well as the contours of the shapes drawn on the ball surface at the beginning and at the end of the exposure [20] (second image); the system first computes the ball motion from γ_b and γ_e, then asks the user to identify the displacement of at least two features on the ball surface (third image), which are easily recognizable. Finally, the same geometric technique we described previously is exploited for recovering spin axis and speed. Note that in this context, the user solves the orientation problem by exploiting prior knowledge about the scene; the feature displacements can also be recovered rather accurately.

and disadvantages of an approach based on blur analysis. Experiments show satisfactory results both in synthetic and real images, especially for translation estimation. Also the 3D spin axis and the angular speed are effectively recovered when the ball's apparent translation is negligible. In fact this scenario, which is not unusual in practice, does not present the orientation problem, can be handled with simple alpha matting techniques, and presents higher tolerance to errors in PSF lengths estimation (which we have found to be quite unreliable). Unfortunately, due to these issues, we are still far from a fully automated approach consistently working in the most general case when the ball is spinning and translating simultaneously; for this purpose, we introduced an user-assisted technique which seems promising for many realistic scenarios.

In a broader view, our technique retrieves 3D information and solves a non-trivial motion estimation problem by exploiting the motion blur in a single image. Although unusual, this approach may result successful in situations where traditional video-based methods fail; target applications include training support and match analysis in sport environments.

References

1. Boracchi, G., Caglioti, V., Giusti, A.: Ball position and motion reconstruction from blur in a single perspective image. In: Inproceedings of ICIAP 2007,Modena. (2007)
2. Boracchi, G., Caglioti, V., Giusti, A.: Single-image 3d reconstruction of ball velocity and spin from motion blur. In: VISAPP 2008, the 3rd International Conference on Computer Vision Theory and Applications 22 - 25 January, 2008 Funchal, Madeira - Portugal. (2008)
3. Fergus, R., Singh, B., Hertzmann, A., Roweis, S.T., Freeman, W.T.: Removing camera shake from a single photograph. In: ACM SIGGRAPH 2006 Papers. (2006)

4. Levin, A.: Blind motion deblurring using image statistics. In Schölkopf, B., Platt, J., Hoffman, T., eds.: Advances in Neural Information Processing Systems 19. MIT Press, Cambridge, MA (2007)
5. Jia, J.: Single image motion deblurring using transparency. In: Inproceedings of CVPR 2007, Minneapolis. (2007)
6. Klein, G., Drummond, T.: A single-frame visual gyroscope. In: Proc. British Machine Vision Conference (BMVC'05). Volume 2., Oxford, BMVA (September 2005) 529–538
7. Levin, A., Fergus, R., Durand, F., Freeman, W.T.: Image and depth from a conventional camera with a coded aperture. ACM Trans. Graph. **26**(3) (2007) 70
8. Rekleitis, I.M.: Steerable filters and cepstral analysis for optical flow calculation from a single blurred image. In: Vision Interface, Toronto (May 1996) 159–166
9. Lin, H.Y., Chang, C.H.: Automatic speed measurements of spherical objects using an off-the-shelf digital camera. In: Mechatronics, 2005. ICM '05. IEEE International Conference on. (10-12 July 2005) 66–71
10. Gopal Pingali, A.O., Jean, Y.: Ball tracking and virtual replays for innovative tennis broadcasts. In: proc. of ICPR 2000 Conference, Washington, DC, USA, IEEE Computer Society (2000) 4152
11. J Ren, J. Orwell, G.J., Xu, M.: A general framework for 3d soccer ball estimation and tracking. In: Proc. of ICIP 2004 Conference. (2004)
12. Jonathan Rubin, Burkhard C. Wuensche, L.C., Stevens, C.: Computer vision for low cost 3-d golf ball and club tracking. In: Proc. of Image and Vision Computing New Zealand. (2005)
13. Reid, I.D., North, A.: 3d trajectories from a single viewpoint using shadows. In: proc. of BMVC 1998 Conference. (1998)
14. Kim, T., Seo, Y., Hong, K.S.: Physics-based 3d position analysis of a soccer ball from monocular image sequences. In: proc of ICCV 1998 Conference. (1998) 721–726
15. Ohno, Y., Miura, J., Shirai, Y.: Tracking players and estimation of the 3d position of a ball in soccer games. In: ICPR. (2000) 1145–1148
16. Caglioti, V., Giusti, A.: Recovering ball motion from a single motion-blurred image. Computer Vision and Image Understanding, in press
17. Bertero, M., Boccacci, P.: Introduction to Inverse Problems in Imaging. Institute of Physics Publishing (1998)
18. Smith, A.R., Blinn, J.F.: Blue screen matting. In: SIGGRAPH '96: Proc. of the 23rd annual conference on Computer graphics and interactive techniques. (1996) 259–268
19. Mishima, Y.: Soft edge chroma-key generation based upon hexoctahedral color space. U.S. Patent 5,355,174 (1993)
20. Caglioti, V., Giusti, A.: On the apparent transparency of a motion blurred object. In: Proc. of ICCV workshop on Photometric Analysis in Computer Vision (PACV) 2007. (2007)
21. Giusti, A., Caglioti, V.: Isolating motion and color in a motion blurred image. In: Proc. of BMVC 2007
22. Yitzhaky, Y., Kopeika, N.S.: Identification of blur parameters from motion-blurred images. In: Proc. SPIE Vol. 2847. (November 1996) 270–280
23. Harris, C., Stephens, M.: A combined corner and edge detector. In: Proceedings of the 4th Alvey Vision Conference,. (1988) 147–151
24. `http://www.blender.org`: Blender 3d modeler
25. Donoho, D.L., Johnstone, I.M.: Ideal spatial adaptation by wavelet shrinkage. Biometrika **81**(3) (1994) 425–455